

High precision measurements of α_s at the future EIC

T. Kutz¹, J. R. Pybus¹, D. W. Upton^{2,3}, C. Cotton², A. Deshpande^{4,5}, A. Deur^{6,*}, W.B. Li^{4,5,7}, D. Nguyen^{6,8}, M. Nycz², X. Zheng²

¹Massachusetts Institute of Technology, Cambridge, MA, USA

²University of Virginia, Charlottesville, VA, USA

³Old Dominion University, Norfolk, VA, USA

⁴Center for Frontiers in Nuclear Science, Stony Brook, NY, USA

⁵Stony Brook University, Stony Brook, NY, USA

⁶Thomas Jefferson National Accelerator Facility, Newport News, VA, USA

⁷The College of William and Mary, Williamsburg, VA, USA

⁸University of Tennessee, Knoxville, TN, USA

Abstract

We present a projection study for the first moments of the inclusive spin structure function $\int g_1(x, Q^2) dx$ for the proton and neutron from simulated doubly-polarized $\vec{e}\vec{p}$ and $\vec{e}\text{-}^3\vec{\text{He}}$ collision data expected from the Electron-Ion collider. For detection and extraction of the neutron spin asymmetries from $\vec{e}\text{-}^3\vec{\text{He}}$ collisions, we used the double-tagging method which significantly reduces the uncertainty over the traditional inclusive method. Using the Bjorken sum rule, the projected results allow us to determine that the QCD coupling at the Z -pole $\alpha_s(M_{Z^0}^2)$ can be measured with a relative precision of 1.3%. This underscores the significance of the EIC for achieving precision determinations of α_s .

1. Introduction

Quantum chromodynamics (QCD) is the quantum field theory (QFT) describing the strong force [1], and one of the main components of the Standard Model (SM) of particle physics. The strength of QCD is characterized by its coupling constant: α_s [2], making it a key parameter of the SM. Accurate knowledge of α_s is important for precisely calculating perturbative QCD (pQCD) series, as it serves as the expansion parameter. However, pQCD series convergence is slow due to the relatively large value of α_s and the renormalon problem [3]. To match the precision required by present-day hadron scattering experiments that aim at testing the SM and exploring beyond-Standard-Model (BSM) physics, the relative uncertainty on α_s needs to be below the % level, lest it dominates the other uncertainties [2, 4]. Yet, achieving such experimental accuracy on α_s is a challenge. The world data compilation by the Particle Data Group results in $\Delta\alpha_s/\alpha_s = 0.85\%$ [5]. This positions α_s as the least precisely known fundamental coupling when compared to the uncertainties on other fundamental couplings: $\Delta\alpha/\alpha = 1.5 \times 10^{-10}$ for the electromagnetic coupling, $\Delta G_F/G_F = 5.1 \times 10^{-7}$ for the weak coupling, and $\Delta G_N/G_N = 2.2 \times 10^{-5}$ for gravity's coupling [5]. Consequently, a large effort is presently being devoted within the QCD community to reduce $\Delta\alpha_s/\alpha_s$ [4].

In this article, we study the accuracy at which α_s can be extracted from the Bjorken sum rule [6, 7] measured at the Electron-Ion Collider (EIC) [8].

We first discuss the extraction of α_s from deep inelastic scattering (DIS) observables, particularly focusing on the Bjorken Sum Rule (BJSR), which is formed from the nucleon spin structure functions $g_1^{p,n}$. Next, we present the simulation of EIC double-polarization data and projection studies on the double-spin asymmetry measurement. The projection is based on three energy settings each of ep and $e\text{-}^3\text{He}$ collisions with an integrated luminosity of 10 fb^{-1} per setting. The polarization is assumed to be 70% for both the electron and the proton (ion) beams. We then present projected results on the BJSR and extraction of α_s (evolved from the measured square 4-momentum transfer Q^2 to the Z^0 mass) and conclusions.

2. Strong coupling from polarized DIS: The Bjorken Sum Rule

The underlying process of DIS, or inclusive inelastic lepton-hadron scattering at large Q^2 and large energy transfer, is elementary lepton-quark scattering. DIS data are sensitive to α_s via violations of the Bjorken scaling, viz through the logarithmic Q^2 -dependence of the nucleon structure functions [9, 10]. At leading order (LO), scaling violations stem from gluon bremsstrahlung radiation emitted by the struck quark of relative momentum x , photon-gluon fusion, and pair creations. At next-to-leading order (NLO), contributions arise also from the quark-photon vertex and quark self-energy. Arguably, DIS structure functions are among the most robust observables for extracting α_s due to their fully inclusive nature,

*Contact author

57 rendering them immune to uncertainties stemming from
58 final-state hadronic corrections.

59 One avenue to obtain α_s from the Q^2 -evolution of the
60 structure functions is by concurrently fitting them (and
61 possibly including other hard process data) [2, 3]. This
62 is a complex endeavor involving global fits based on the
63 DGLAP evolution equations [11, 12, 13]. It also requires
64 modeling non-perturbative inputs such as the quark and
65 gluon distribution functions, and higher-twist (HT) cor-
66 rections if data from low- Q^2 or high- x regions are used as
67 inputs.

68 In the fitting method described above, data from
69 double-polarization DIS contributed minimally due to
70 their scarcity at the necessary high Q^2 and their relatively
71 large uncertainty compared to unpolarized data. Even
72 with the EIC, polarized data will still impact minimally
73 the extraction of α_s from global fits. This is because po-
74 larized absolute measurements needed, e.g., for g_1 have
75 necessarily lower statistics and possess extra uncertainties
76 such as those from polarimetries. Since the Q^2 (viz α_s)
77 dependence of polarized and unpolarized parton distri-
78 bution functions (PDF) are similar, these issues lessen the
79 impact of polarized data on α_s extracted from global fits.
80 Relative measurements (asymmetries) have the same is-
81 sues and often employ PDFs as input to correct for unpo-
82 larized contributions, with a specific α_s value assumed to
83 extract these PDFs thereby biasing its extraction. Further-
84 more, asymmetries have a suppressed Q^2 -dependence.
85 For these reasons, they are even less suited.

86 On the other hand, double-polarization observables
87 could contribute in a unique way through the Q^2 -
88 evolution of the first moments of spin structure func-
89 tions [14],

$$90 \quad \Gamma_1(Q^2) \equiv \int_0^{1^-} g_1(Q^2, x) dx. \quad (1)$$

91 The integration in x simplifies the formalism and consoli-
92 dates the statistical fluctuations in the data. Furthermore,
93 there is no model-dependence aside from the generic as-
94 sumption of $SU(3)_F$ mass symmetry, since the leading-
95 twist (LT) non-perturbative inputs to Γ_1 's Q^2 -evolution
96 are the measured axial charges $a_0, a_3(\equiv g_A)$ and a_8 [14].
97 However, a hurdle is the unreachable low x part of the
98 integral. The lowest x -value reachable depends on the
99 beam energy, how forward the scattered leptons can be
100 measured, and the minimum Q^2 value tolerable for data
101 interpretation. The upcoming Electron-Ion Collider will
102 broaden the scope of double-polarization high-precision
103 DIS measurements to encompass lower x regions previ-
104 ously unexplored.

105 In that context, it is beneficial to consider the isovector
106 (proton minus neutron, p-n) combination $\Gamma_1^{p-n} \equiv \int_0^{1^-} (g_1^p -$
107 $g_1^n) dx$, called the Bjorken integral. It provides one of the
108 two components of the BJSR [6, 15] that links Γ_1^{p-n} to g_A
109 for $Q^2 \rightarrow \infty$:

$$110 \quad \Gamma_1^{p-n}(Q^2)|_{Q^2 \rightarrow \infty} = \frac{g_A}{6}. \quad (2)$$

111 At finite Q^2 values, the pQCD processes mentioned above
112 introduce an α_s -dependence:

$$\begin{aligned} 113 \quad \Gamma_1^{p-n}(\alpha_s) &= \Gamma_1^{p-n}(Q^2) = \sum_{\tau>0} \frac{\mu_{2\tau}^{p-n}(\alpha_s)}{Q^{2\tau-2}} \\ 114 \quad &= \frac{g_A}{6} \left[1 - \frac{\alpha_s(Q^2)}{\pi} - 3.58 \left(\frac{\alpha_s(Q^2)}{\pi} \right)^2 \right. \\ 115 \quad &\quad \left. - 20.21 \left(\frac{\alpha_s(Q^2)}{\pi} \right)^3 - 175.7 \left(\frac{\alpha_s(Q^2)}{\pi} \right)^4 - \right. \\ 116 \quad &\quad \left. (\sim 893.38) \left(\frac{\alpha_s(Q^2)}{\pi} \right)^5 + \mathcal{O}((\alpha_s)^6) \right] + \sum_{\tau>1} \frac{\mu_{2\tau}^{p-n}(\alpha_s)}{Q^{2\tau-2}}, \quad (3) \end{aligned}$$

117 where the $\mu_{2\tau}$ are the coefficients of the HT expansion.
118 Here, the series coefficients for the LT μ_2 are calculated in
119 the $\overline{\text{MS}}$ renormalization scheme (RS) [16, 17, 18] and for
120 $n_f = 3$ quark flavors. Results on α_s extracted from Eq. (3)
121 are therefore in $\overline{\text{MS}}$ RS, which is the standard one for re-
122 porting α_s [5]. Since we aim at estimating the uncertainty
123 $\Delta\alpha_s/\alpha_s$, n_f may be kept fixed. For the actual extraction of
124 α_s from data, quark threshold effects should be accounted
125 for both in the α_s series and the BJSR series, Eq. (3). Quark
126 threshold corrections for the latter are presently known at
127 NNLO [19]. We assume that they will be available for
128 higher order by the time EIC delivers the Bjorken sum
129 data. Finally and importantly, the determination of α_s us-
130 ing Eq. (3) does not assume α_s , directly or indirectly in
131 contrast to other approaches that, e.g., requires PDF in-
132 puts such as ΔG which are determined assuming a specific
133 value of α_s .

134 Γ_1^{p-n} displays a relatively simple LT Q^2 -evolution, known
135 to a higher order than for the individual nucleon cases.
136 This is crucial since the truncation of a pQCD series typi-
137 cally creates one of the dominant uncertainties when ex-
138 tracting α_s [4]. Equation (3) shows that the pQCD ap-
139 proximant of the BJSR is known at N⁴LO (order α_s^4), with
140 an N⁵LO estimate. The same accuracy is available for α_s ,
141 for which the pQCD approximation has been calculated
142 at five loops in the $\overline{\text{MS}}$ RS [20], i.e., up to β_4 in the QCD β -
143 series [2]. Additionally, the LT non-perturbative input is
144 precisely measured, $g_A = 1.2762(5)$ [5], and HT are known
145 to be small for Γ_1^{p-n} [21]. In Eq. (3) we only wrote the Q^2 -
146 dependence of the LT, μ_2 . The twist-4 term, μ_4 has been
147 phenomenologically determined [21, 22, 23]. In that pro-
148 cedure, however, an α_s was assumed. Thus, using the phe-
149 nomenological value would bias our extraction of the cou-
150 pling toward the α_s . Here, we will ignore μ_4 and other HT
151 since they are suppressed at the relatively high Q^2 covered
152 by EIC.

153 One can obtain α_s from $\Gamma_1^{p-n}(Q^2)$ in two ways: The first is
154 to solve Eq. (3) for α_s , for each Γ_1^{p-n} data point. This maps
155 the Q^2 -dependence of α_s but the method is inaccurate be-
156 cause it relies on an absolute determination of $\Gamma_1^{p-n}(Q^2)$: At
157 LO and assuming a reasonable precision of 10% on Γ_1^{p-n} ,
158 $\Delta\alpha_s \simeq 0.1\pi$, that is $\Delta\alpha_s/\alpha_s \gtrsim 100\%$ for $Q^2 \gtrsim 3 \text{ GeV}^2$. The

159 second way, employed here, is more accurate and involves
160 fitting the Q^2 -evolution of $\Gamma_1^{p-n}(Q^2)$ [24].

161 3. Projection for Double-Spin Asymmetries

162 We now discuss the generation process of simulated
163 EIC data and the expected uncertainties on the double-
164 spin asymmetries.

165 3.1. Proton DIS simulation

166 Neutral-current ep DIS events were generated using the
167 DJANGO 4.6.10 [25, 26] event generator, for three EIC
168 ep collision energy settings: 5×41 GeV, 10×100 GeV, and
169 18×275 GeV [27].

170 Full details of the input parameters used in the DJAN-
171 GOH generation can be found in the appendix of Ref. [28].
172 The simulated yields were scaled to provide an estimate
173 for the total event counts that correspond to an integrated
174 luminosity of 10 fb^{-1} for each combination of energy set-
175 ting and hadron polarization (longitudinal and trans-
176 verse).

177 The operation time that corresponds to the 10 fb^{-1} in-
178 tegrated luminosity varies with energy, which are 27.3,
179 2.7, and 7.8 months, respectively, for the 5×41 GeV, 10×100
180 GeV, and 18×275 GeV settings [8, 27]. In real running, the
181 beam time can be split between longitudinal and trans-
182 verse hadron polarization settings. Given that A_1 is a
183 mainly longitudinal quantity, the relative ratio can be op-
184 timized in favor of longitudinal running.

185 It is also worth noting that the lowest energy EIC opera-
186 tions of ep and e - ^3He pose significant technical challenges,
187 and solutions are being developed [29]. Depending on
188 the engineering and construction feasibility of the final-
189 ized accelerator design, a small adjustment is anticipated
190 for the lowest collision energy setting. This will result in
191 a shift in the Q^2 and x coverage.

192 We chose to simulate events as detected by the EIC
193 Comprehensive Chromodynamics Experiment (ECCE)
194 detector [30]. Other proposed EIC detector designs
195 should yield very similar results in the context discussed
196 here. In fact, the ATHENA [31] and ECCE configurations
197 have now been combined in the ePIC design. Despite dif-
198 ferences in apparatus details, the overall kinematic range
199 and achievable precision are expected to be similar. Gen-
200 erated events were passed through ECCE's GEANT4 [32]
201 based full detector simulation framework to account for
202 the impact of detector resolution, efficiency, and accep-
203 tance. The events from the output were used as pseudo-
204 data to estimate event rates for this analysis. DIS events
205 were selected using the following criteria based on the ex-
206 pected performance of the ECCE detectors:

- 207 • DIS kinematics $Q^2 > 2 \text{ GeV}^2$ and invariant mass $W >$
208 $\sqrt{10} \text{ GeV}$
- 209 • The scattered electron's energy $E'_e > 2 \text{ GeV}$ and
210 pseudo-rapidity $\eta_e > -3.5$, to isolate regions of high
211 detector efficiency

- 212 • The inelasticity of the scattering event $0.01 < y < 0.95$,
213 to avoid regions of poor reconstruction/resolution
214 and reduce the large photoproduction background in
215 the high- y region.

216 Selected events were binned in two dimensions by the re-
217 constructed values of x and Q^2 .

218 One important feature of DJANGO is that it calculates
219 not only the vertex-level scattering for an event but also
220 details of initial- and final-state electromagnetic and elec-
221 troweak radiation for the scattering event, which would
222 distort the event from Born-level kinematics. Further-
223 more, the energy loss of particles due to passing through
224 material and detector resolution effects add further distor-
225 tion. To correct for the sizable bin migration due to these
226 effects, the binned events were unfolded to the Born-level
227 distribution in x and Q^2 with a 4-iteration Bayesian un-
228 folding algorithm using the RooUnfold [33] framework,
229 trained with the Born-level and reconstructed values in
230 the pseudo-data. The unfolding algorithm provided an
231 estimate of the increase of uncertainties resulting from the
232 correction for bin migration and QED radiative effects, al-
233 lowing for the estimation of both statistical and systematic
234 uncertainties on the binned yields.

235 3.2. Neutron DIS simulation

236 The neutron spin asymmetry information is tradition-
237 ally extracted from the inclusive measurement of elec-
238 trons scattering off light nuclei such as deuteron or ^3He .
239 Since the neutron spin accounts for almost 90% of ^3He
240 spin, the latter is preferred for neutron spin measurement.
241 However, the extraction introduces a sizeable systematic
242 uncertainty due to our limited understanding of nuclear
243 effects. The far-forward detector region at EIC provides a
244 unique opportunity for tagging measurements in which
245 we can detect both spectator protons in helium. This
246 double-tagging method selects the signal for scattering off
247 a quasi-free neutron in ^3He , thereby suppressing the nu-
248 clear correction uncertainties [34].

249 The DJANGO event generator was used to produce
250 a sample of neutral-current DIS events from ^3He , using
251 similar input parameters to the proton-scattering case. As
252 DJANGO does not include the effects of Fermi motion,
253 the spectator nucleons were separately generated and
254 added to the event sample. The distributions of the spec-
255 tator nucleons were simulated using the convolution ap-
256 proximation for nuclear structure functions in the Bjorken
257 limit [35], using the ^3He ground-state model of Ref. [36],
258 the light-front formalism of Ref. [34], and the structure
259 functions of Refs. [37, 38].

260 DIS e - ^3He events were generated for three EIC energy
261 settings: 5×41 GeV/nucleon, 10×100 GeV/nucleon, and
262 18×166 GeV/nucleon, and were scaled to an integrated
263 luminosity of 10 fb^{-1} for each energy and ^3He polariza-
264 tion (longitudinal and transverse) setting. The generated
265 events were passed through the Geant4 simulation and

analysis framework. The first step to selecting the double spectator tagged sample is applying identical cuts on the reconstructed electron variables as applied in the ep case (see Section 3.1).

The criteria for selecting the spectator protons require the integrated detector stack in the far-forward region (close to the downstream hadron beamline) to detect both remaining protons simultaneously such that the electron interacting with the quasi-free neutron in the ^3He is favored. This is also referred to as the “double-tagging” technique, see further detail in Ref. [39].

Nuclear effects were minimized by requiring $|\vec{p}_{s1} + \vec{p}_{s2}| < 0.1$ GeV, where $\vec{p}_{s1,2}$ are the 3-momenta of the two spectator protons, see Ref. [39] for details.

3.3. A_1 extraction

The virtual photon asymmetry for electron scattering off a hadron of spin-1/2 is defined as

$$A_1(x, Q^2) \equiv \frac{\sigma_{1/2} - \sigma_{3/2}}{\sigma_{1/2} + \sigma_{3/2}}, \quad (4)$$

where $\sigma_{1/2(3/2)}$ is the total virtual photo-absorption cross section for the nucleon with a projection of 1/2(3/2) for the total spin along the direction of the photon momentum. At high enough Q^2 that satisfies $\gamma \ll 1$, where $\gamma^2 = (2Mx)^2/Q^2$ with M the nucleon mass, $A_1 \approx g_1/F_1$. Thus, we can form the spin structure function g_1 by combining measured A_1 with a world parameterization of the unpolarized structure function F_1 .

In practice, A_1 is extracted from the measured longitudinal (A_{\parallel}) and transverse electron asymmetries (A_{\perp}):

$$A_{\parallel} = \frac{\sigma_{\downarrow\uparrow} - \sigma_{\uparrow\uparrow}}{\sigma_{\downarrow\uparrow} + \sigma_{\uparrow\uparrow}} \quad \text{and} \quad A_{\perp} = \frac{\sigma_{\downarrow\Rightarrow} - \sigma_{\uparrow\Rightarrow}}{\sigma_{\downarrow\Rightarrow} + \sigma_{\uparrow\Rightarrow}},$$

where the \downarrow, \uparrow represents the spin of the longitudinally polarized electron anti-parallel (parallel) to beam direction, and the \uparrow, \Rightarrow the spin of the longitudinally or transversely polarized hadron. The relation between A_1 , A_{\parallel} and A_{\perp} is

$$A_1 = \frac{A_{\parallel}}{D(1 + \eta\xi)} - \frac{\eta A_{\perp}}{d(1 + \eta\xi)}, \quad (5)$$

where [40, 41]

$$D = \frac{y(2-y)(2+\gamma^2y)}{(2(1+\gamma^2)y^2 + (4(1-y) - \gamma^2y^2)(1+R))} \quad (6)$$

$$d = \sqrt{4(1-y) - \gamma^2y^2} D / (2-y) \quad (7)$$

$$\eta = \gamma(4(1-y) - \gamma^2y^2) / (2-y) / (2+\gamma^2y) \quad (8)$$

$$\xi = \gamma(2-y) / (2+\gamma^2y), \quad (9)$$

which are kinematic factors, except $R \equiv \sigma_L/\sigma_T$, which is the ratio of the longitudinal to transverse virtual photon absorption cross sections. The world data fit [42] was used for R [43].

For both the proton and ^3He cases, the unfolded event yields in each bin of x and Q^2 were used to estimate the yield-related uncertainties on the spin asymmetries:

$$\delta A_{\parallel,\perp} \simeq \frac{\delta N}{NP_e P_N} \quad (10)$$

where N is the total event yield in the bin, δN is the overall uncertainty on that yield, and P_e and P_N are the polarizations of the electron and ion beam respectively, taken to be $(70 \pm 1)\%$. Equation (10) yields conservative uncertainties since they would be smaller if the asymmetry is large. The uncertainties $\delta A_{\parallel,\perp}$ were then propagated into the total uncertainty on A_1 . The kinematic coverage and uncertainties for A_1^p and A_1^n are shown in Fig. 1. Note that the asymmetry measurements for both parallel (A_{\parallel}) and perpendicular (A_{\perp}) will be performed, owing to EIC’s capability of providing transversely polarized hadron beams.

4. Extraction of α_s from the simulated EIC data

4.1. Formation of g_1 and its moments

Once the projected results on the proton and the neutron A_1^p and A_1^n were produced from the simulation, these were multiplied by F_1^p and F_1^n obtained from a global fit [44] to provide the projected results on g_1^p and g_1^n . Specifically, both the central value and the uncertainty in $F_1^{p,n}$ were evaluated using the grid JAM22-STF_proton [44] and its replicas. While we expect that future data will provide a reasonable description of the $F_1^{p,n}$ themselves, the uncertainty of the projection on the polarized quantities is dominated by the statistical uncertainty in the asymmetry projection, and thus using a world fit of the F_1 ’s should be sufficient for the present work.

The projected results on g_1^p and g_1^n were then integrated over the available x range to obtain the integrals $\int g_1^p dx$ and $\int g_1^n dx$. For the low W (high x) region, either not covered by the EIC simulated data or where the EIC projection provides large statistical uncertainty, we used a parameterization [45] that provides a good description of most of the existing world double-polarization data. In other words, the integral of Eq. (1) was formed as:

$$\Gamma_1^{\text{proj.}}(Q^2) = \int_{x_{\text{min}}}^{x_{\text{param.}}} g_1^{\text{proj.}}(Q^2, x) dx + \int_{x_{\text{param.}}}^{1^-} g_1^{\text{param.}}(Q^2, x) dx.$$

The uncertainty of the full integral accounts for the statistical uncertainties of the projection and model uncertainty, and is evaluated by varying the model inputs. The projected values of $\Gamma_1^{p,n}$ for each Q^2 and the coverage of EIC projection vs. model usage are summarized in Table 1.

The finite beam energies and the DIS requirement of minimal Q^2 values limit the experimental reach at low x . The unmeasured contribution, $\Gamma_1^{\text{low-}x} \equiv \int_0^{x_{\text{min}}} (g_1^p - g_1^n) dx$, with x_{min} being the lowest x value covered by the EIC (see Table 1) was estimated from the difference between the simulated partial integral and the full Bjorken integral

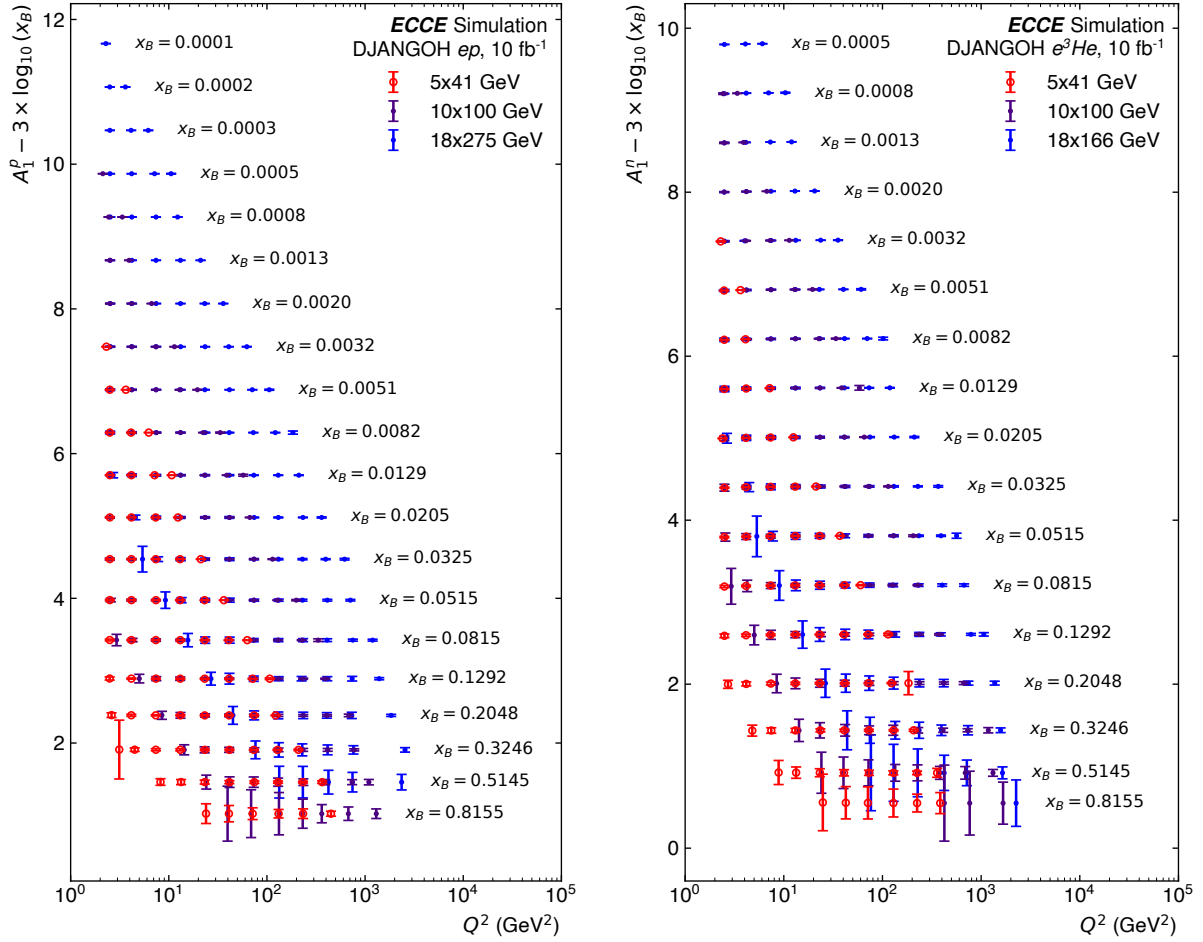


Figure 1: Coverage for A_1^n and A_1^p using an integrated luminosity of 10 fb^{-1} for each of the longitudinally and transversely polarized hadron beam per energy settings. Three energy settings were used for each of ep and $e^3\text{He}$ collisions. Projections for different x values are by $3 \times \log_{10}(x)$ for clarity. The error bars are statistical uncertainties.

$Q^2[\text{GeV}^2]$	x_{min}	$x_{\text{p param}}$	$x_{\text{n param}}$	Γ_1^{p-n}
2.37	0.0006	0.046	0.060	$0.1817 \pm 16 \pm 06$
4.22	0.0006	0.105	0.176	$0.1935 \pm 17 \pm 10$
7.50	0.0010	0.160	0.263	$0.1949 \pm 17 \pm 13$
13.34	0.0016	0.506	0.506	$0.1945 \pm 21 \pm 23$
23.71	0.0025	0.807	0.807	$0.1901 \pm 20 \pm 23$
42.17	0.0100	0.802	0.802	$0.1621 \pm 19 \pm 21$
74.99	0.0100	0.915	0.915	$0.1632 \pm 19 \pm 19$

Table 1: Projected integrals $\Gamma_1^{p,n}$, along with the minimum x covered by the EIC projection, the x_{param} above which the model parameterization was used for proton (third column) and neutron (fourth column), and the resulting integrals. The first uncertainty on the integral includes statistical uncertainty and experimental effects (detector smearing, bin migration, and unfolding), while the second uncertainty corresponds to that due to both electron and hadron beam polarimetry.

be used for an accurate determination of the low x uncertainty, rather than the central value of α_s that is immaterial for this work. For the analysis of the future EIC data, the missing low x part can be estimated using Regege theory, as was done in [21], for which parameters are expected to improve thanks to both EIC and dedicated JLab 12 GeV experiments [46]. Once the value of the missing low x part was estimated, its contribution to the uncertainty $\Delta\alpha_s/\alpha_s$ was evaluated using the procedure outlined in [21]: $\Delta_Q \Gamma_1^{\text{low}-x} = \left(\frac{d\Gamma_1^{p-n}}{dQ^2}\right) \left(\frac{\Delta Q^2}{2}\right) \left(\frac{\Gamma_1^{\text{low}-x}}{\Gamma_1^{p-n}}\right)$, with ΔQ^2 as the Q^2 bin size, and the derivative $\frac{d\Gamma_1^{p-n}}{dQ^2}$ calculated based on the theoretical expectation for the $\Gamma_1^{p-n} Q^2$ -dependence. The unmeasured part of Γ_1^{p-n} and $\Delta_Q \Gamma_1^{\text{low}-x}$ are given in Table 2.

4.2. Extraction of α_s

To extract $\alpha_s(M_{Z_0}^2)$, the simulated $\Gamma_1^{p-n}(Q^2)$ values are fitted using Eq. (3). The key free parameter in the fit is the QCD scale Λ_s [2]. Knowing it is sufficient to provide the value of $\alpha_s(M_{Z_0}^2)$. For instance, at LO, $\alpha_s(Q^2) =$

$Q^2[\text{GeV}^2]$	x_{\min}	$\int_0^{x_{\min}} g_1^{p-n} dx$	$\Delta_Q \Gamma_1^{\text{low-}x}$
2.37	0.0006	-15.74×10^{-3}	0.60×10^{-3}
4.22	0.0006	-15.98×10^{-3}	0.30×10^{-3}
7.50	0.0010	-10.54×10^{-3}	0.12×10^{-3}
13.34	0.0016	-5.57×10^{-3}	0.04×10^{-3}
23.71	0.0025	1.11×10^{-3}	0.00×10^{-3}
42.17	0.0100	31.50×10^{-3}	0.13×10^{-3}
74.99	0.0100	32.26×10^{-3}	0.11×10^{-3}

Table 2: Unmeasured low x part of Γ_1^{p-n} . The fourth column provides the uncertainty on the normalized Q^2 -dependence of the missing part (third column), see main text.

$\frac{12\pi}{(11n_c - 2n_f)\ln(Q^2/\Lambda_s^2)}$, with n_c and n_f the numbers of quark colors and flavors, respectively. From the fit, $\Delta\Lambda_s$ is derived, which allows the computation of $\Delta\alpha_s(M_{Z_0}^2)$, the quantity of interest in this study.

The other free parameter in the fit is g_A . Despite being well-measured, we allow it to vary freely to accommodate potential offsets from the systematic uncertainties in the Γ_1^{p-n} expected in the real data.

Generally, the total uncertainty is minimized by optimizing the number of low- Q^2 points versus high- Q^2 points. The former provides higher sensitivity to α_s and minimal fit uncertainty but increases truncation uncertainty. The latter becomes asymptotically insensitive to α_s and exhibits increased uncertainties at low x . For this work, we found that including all simulated data, viz. fitting over a range of $2.4 < Q^2 < 75 \text{ GeV}^2$, is optimal.

Using N⁴LO and LT, our best-fit yields $\Delta\alpha_s/\alpha_s = [\pm 8.3(\text{fit}) \pm 6.4(\text{trnc})] \times 10^{-3}$, where the first uncertainty arises from the fit, and the second from the truncation of the pQCD series, Eq. (3). The uncertainty of the fit accounts for the expected statistical uncertainty of the measurement, experimental effects (detector smearing, bin migration, and unfolding), the missing low x contribution, and the parameterizations. The truncation uncertainty is estimated by re-fitting the data with the Γ_1^{p-n} and α_s approximants at N⁵LO and taking the difference $|\Lambda_s^{(5)} - \Lambda_s^{(4)}|/2$ as the truncation error. (Here the superscript (4) or (5) denotes the order for the series of Γ_1^{p-n} and α_s .)

To account for the beam polarization uncertainty, we utilized a Monte Carlo-based method. First, we generated pseudo data for $g_1^{p,n}$ of each beam energy settings i , with the centroid given by the parameterizations as described in Section 4.1:

$$g_{1,i}^{\text{MC,syst}} = g_1^{\text{centroid}}(1 + r_i), \quad (11)$$

where r_i is a random number following a normal distribution of standard deviation 0.02 to account for the 2% combined uncertainty of the two beam polarimetry, with $i = 1, 2, \dots, 6$ standing for the two beam types (p or ^3He) and the three energy settings. The r_i is independent (uncorrelated) among the six settings. The generated g_1 are then combined to form Γ_1^{p-n} following the procedure of

Section 4.1. In the region where two beam energies overlap, the systematic uncertainty is combined following the same statistical weighting as the simulated physics data. The resulting uncertainty on Γ_1^{p-n} is shown in Table 1. The Γ_1^{p-n} from each Monte-Carlo event is then fed to the α_s fitting procedure with all other uncertainties (statistical, truncation, low x) set to zero, such that fluctuations in the fitted α_s result would represent the effect from the beam polarization uncertainty. This yields an uncertainty on α_s of 0.78%. Another source of systematic uncertainty is radiative corrections, which were taken into account in the unfolding procedure described in Section 3.1.

Adding all uncertainties in quadrature, we obtain a precision on α_s of $\Delta\alpha_s/\alpha_s = 1.3\%$. The simulated $\Gamma_1^{p-n}(Q^2)$ and best fits are shown in Fig. 2. Also shown is the missing low x contribution (lower panel). Notably, it becomes negative for $Q^2 \lesssim 23 \text{ GeV}$. There is no *a-priori* reason to expect the low x missing contribution to be positive since the BJSR components need not be positive quantities and since the value of the missing low x part depends on experimental conditions. Yet, it is likely that the negative low x contribution at the lower Q^2 stems from uncertainties in the PDFs used to estimate the Γ_1 . In fact, the missing contribution is small since $x_{\min} \sim 10^{-3}$. A Regge theory estimate [47] predicts it to be about 2% of the expected full Γ_1^{p-n} . Thus, PDF systematics may affect the sign of the missing contribution if the partial Γ_1^{p-n} integral is overestimated by a few %. At larger Q^2 , the missing low x part is larger, about 20% using [47], so its sign is not affected by PDF uncertainties. The expected uncertainty on α_s , shown in Fig. 3, provides a competitive level of precision compared with the current 1.7% uncertainty derived from DIS world data, primarily obtained through global PDF fits of unpolarized and polarized structure functions [5]. Another important uncertainty at low x is the uncertainty in determining the relative luminosity difference between two spin states of the longitudinally polarized electron beam (parallel and antiparallel to beam direction). According to Ref. [27], the EIC physics program requires this uncertainty to be below 10^{-5} to benefit from the statistics of EIC, given the spin asymmetry at low x is already at the 10^{-4} level. The research and development effort of the ePIC collaboration is currently ongoing to achieve this design objective.

4.3. Discussion

The truncation uncertainty being important, we explored using the Principle of Maximum Conformality (PMC) method [49] to reduce that uncertainty. The PMC optimizes a perturbative approximant, thereby allowing for a more accurate determination of α_s from the corresponding observable. The PMC extends the well-known Brodsky-Lepage-Mackenzie method [50], which optimizes perturbative predictions by summing all β -terms into $\alpha_s(Q^2)$. The PMC series for $\Gamma_1^{p-n}(Q^2)$ is calculated in [51]. In this series, each N ^{n} LO order is characterized by a specific scale, Q_n^2 , that matches the vir-

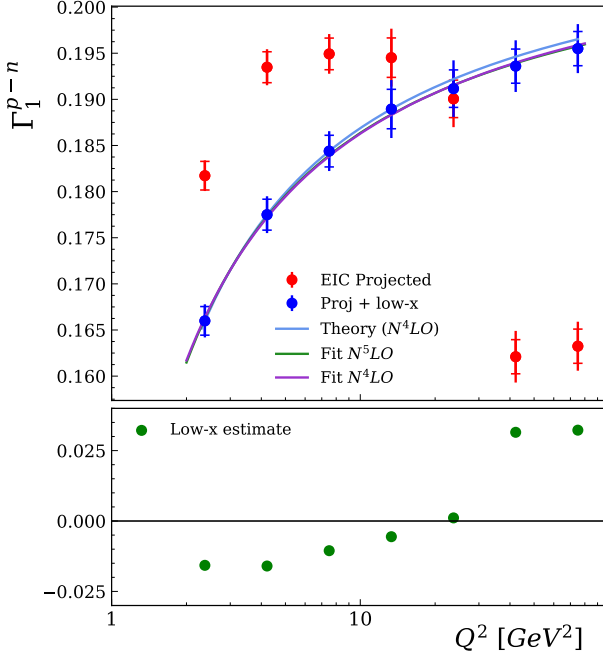


Figure 2: The Bjorken sum Γ_1^{p-n} vs Q^2 . The partial moment integrated over the x -coverage of the EIC and the high- x region from the parameterization is shown as red solid circles. The blue circles show the full integral, viz also including the low x contribution (green solid circles in the lower panel). The inner error bars comprise the uncertainty from statistical and experimental effects (detector smearing, bin migration, and unfolding), and the outer error bar includes in addition (quadratic) the systematic uncertainty from beam polarimetry. The light-blue curve shows the expected $\Gamma_1^{p-n}(Q^2)$ calculated at N⁴LO with α_s at 5-loop. The (nearly indistinguishable) green and purple curves are the N⁵LO, 5-loop, and N⁴LO, 5-loop, fits of the full integral, respectively. We do not show the uncertainty on the unmeasured low x contribution (green circle) since it is not directly relevant to the uncertainty $\Delta\alpha_s/\alpha_s$. The relevant contribution from low x to this uncertainty is given in Table 2.

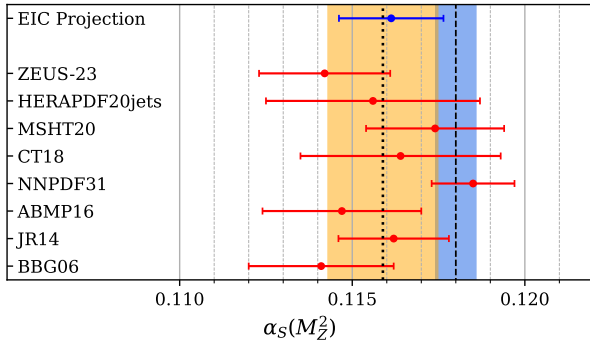


Figure 3: Expected total uncertainty on α_s from this study compared with existing results from DIS world data [5, 48]. The Particle data group [5] average of DIS PDF fits is shown as the golden band, while the world average combining all data and lattice QCD results is shown as the blue band.

improvement in truncation uncertainty.

The BJSR is just one method to determine α_s . Other methods, such as global PDF fits, are also viable at the EIC and should also significantly enhance our determination of α_s using DIS data. Additionally, the optimal range of the fit requires the lowest Q^2 -point, which means that EIC data can be fruitfully complemented by lower Q^2 data with reasonably low x coverage, such as from the possible energy upgrade of JLab. The combination of EIC and JLab data at 22 GeV could potentially yield $\Delta\alpha_s/\alpha_s = 0.6\%$ [52].

It is worth noting that at the EIC, the neutron spin structure could be measured using a polarized deuteron beam. The extraction of the neutron spin structure from inclusive DIS (via eD) is generally simpler and more accurate than for $e^{-3}\text{He}$ [35].

It is understood that preserving the polarization of the polarized deuteron in a circular storage ring is challenging and is beyond the scope of the planned spin rotation capabilities of the EIC. Currently, the development of a polarized deuteron beam is not included in the EIC project R&D effort. It is expected that the experience gained from the polarized ³He beam (projected to be optional on day one), will directly benefit the development of the deuteron beam and polarimetry [27]. The polarized deuteron beam will be available in the form of a future upgrade to the EIC project.

5. Conclusion

The BJSR offers several advantages for an experimental extraction of α_s . It has the robustness of inclusive data, the simplest pQCD evolution (the x -dependence is integrated out and the isospin nature of the BJSR fully or partially suppresses contributions from difficult quantities such as ΔG or coherent reactions), and crucially is model-independent: the sum rule encapsulates the non-perturbative part of the reaction into the well-measured axial charge g_A . The missing low x issue, which is often a significant challenge in studies involving moments, is by design minimal in the case of the EIC. A realistic simulation of EIC data demonstrates that the BJSR can yield $\alpha_s(M_Z^2)$ with an accuracy of approximately $\Delta\alpha_s/\alpha_s \simeq 1.3\%$. This result compares well with the best current extractions of α_s from experimental data. Furthermore, independent methods to accurately determine α_s will be possible using other types of EIC data, e.g., inclusive neutral and charged current reactions studied in [53]. These approaches will achieve a $\Delta\alpha_s/\alpha_s$ below the percentage level, which would make the EIC a key contributor to the global extraction of α_s .

Acknowledgements This material is based upon work supported by the U.S. Department of Energy (DOE), Office of Science, Office of Nuclear Physics under contract DE-AC05-06OR23177. W.B. Li and A. Deshpande were supported by the U.S. DOE Award DE-1020FG02-05ER41372

537 and the Center for Frontiers in Nuclear Science (CFNS),
538 Stony Brook University. The work of D.W. Upton, C. Cot-
539 ton, M. Nycz, and X. Zheng was supported by the U.S.
540 DOE Award DE-SC0014434. Jefferson Science Associates
541 LLC operates the Thomas Jefferson National Accelerator
542 Facility for the DOE under contract DE-AC05-84ER40150,
543 mod. # 175. The work of J.R. Pybus and M. Nycz was sup-
544 ported in part by the EIC² Center fellowship at Jefferson
545 Lab. We also extend our gratitude to Katarzyna Wich-
546 mann and Barak Schmookler for their comments, which
547 have greatly enhanced the quality of this paper.

548 References

- 549 [1] Franz Gross et al. 50 Years of Quantum Chromodynamics. *Eur.*
550 *Phys. J. C*, 12 2022.
- 551 [2] Alexandre Deur, Stanley J. Brodsky, and Craig D. Roberts. QCD
552 Running Couplings and Effective Charges. 3 2023.
- 553 [3] Alexandre Deur, Stanley J. Brodsky, and Guy F. de Teramond. The
554 QCD Running Coupling. *Nucl. Phys.*, 90:1, 2016.
- 555 [4] D. d’Enterria et al. The strong coupling constant: State of the art
556 and the decade ahead. 3 2022.
- 557 [5] P. A. Zyla et al. Review of Particle Physics. *PTEP*, 2020(8):083C01,
558 2020.
- 559 [6] J. D. Bjorken. Applications of the Chiral $U(6) \times (6)$ Algebra of Cur-
560 rent Densities. *Phys. Rev.*, 148:1467–1478, 1966.
- 561 [7] B. Adeva et al. Next-to-leading order qcd analysis of the spin struc-
562 ture function g_1 . *Phys. Rev. D*, 58:112002, Oct 1998.
- 563 [8] A. Accardi et al. Electron Ion Collider: The Next QCD Frontier:
564 Understanding the glue that binds us all. *Eur. Phys. J. A*, 52(9):268,
565 2016.
- 566 [9] J.D. Bjorken and Emmanuel A. Paschos. Inelastic Electron Proton
567 and gamma Proton Scattering, and the Structure of the Nucleon.
568 *Phys. Rev.*, 185:1975–1982, 1969.
- 569 [10] R. P. Feynman. The behavior of hadron collisions at extreme ener-
570 gies. *Conf. Proc. C*, 690905:237–258, 1969.
- 571 [11] V. N. Gribov and L. N. Lipatov. Deep inelastic e p scattering in
572 perturbation theory. *Sov. J. Nucl. Phys.*, 15:438–450, 1972.
- 573 [12] Guido Altarelli and G. Parisi. Asymptotic Freedom in Parton Lan-
574 guage. *Nucl. Phys. B*, 126:298–318, 1977.
- 575 [13] Yuri L. Dokshitzer. Calculation of the Structure Functions for Deep
576 Inelastic Scattering and e+ e- Annihilation by Perturbation Theory
577 in Quantum Chromodynamics. *Sov. Phys. JETP*, 46:641–653, 1977.
- 578 [14] Alexandre Deur, Stanley J. Brodsky, and Guy F. De Teramond. The
579 Spin Structure of the Nucleon. 7 2018.
- 580 [15] J. D. Bjorken. Inelastic Scattering of Polarized Leptons from Polar-
581 ized Nucleons. *Phys. Rev. D*, 1:1376–1379, 1970.
- 582 [16] A. L. Kataev. The Ellis-Jaffe sum rule: The Estimates of the next
583 to next-to-leading order QCD corrections. *Phys. Rev. D*, 50:R5469–
584 R5472, 1994.
- 585 [17] A. L. Kataev. Deep inelastic sum rules at the boundaries be-
586 tween perturbative and nonperturbative QCD. *Mod. Phys. Lett. A*,
587 20:2007–2022, 2005.
- 588 [18] P. A. Baikov, K. G. Chetyrkin, and Johann H. Kuhn. Order α ⁴(s)
589 QCD Corrections to Z and tau Decays. *Phys. Rev. Lett.*,
590 101:012002, 2008.
- 591 [19] Johannes Blümlein, Giulio Falcioni, and Abilio De Freitas. The
592 Complete $O(\alpha_s^5)$ Non-Singlet Heavy Flavor Corrections to the
593 Structure Functions $g_{1,2}^{ep}(x, Q^2)$, $F_{1,2,L}^{ep}(x, Q^2)$, $F_{1,2,3}^{v(\bar{v})}(x, Q^2)$ and the
594 Associated Sum Rules. *Nucl. Phys. B*, 910:568–617, 2016.
- 595 [20] B. A. Kniehl, A. V. Kotikov, A. I. Onishchenko, and O. L. Veretin.
596 Strong-coupling constant with flavor thresholds at five loops in the
597 anti-MS scheme. *Phys. Rev. Lett.*, 97:042001, 2006.
- 598 [21] A. Deur, Y. Prok, V. Burkert, D. Crabb, F. X. Girod, K. A. Grif-
599 fioen, N. Guler, S. E. Kuhn, and N. Kvaltine. High precision de-
600 termination of the Q^2 evolution of the Bjorken Sum. *Phys. Rev. D*,
601 90(1):012009, 2014.
- 602 [22] A. Deur et al. Experimental determination of the evolution of the
603 Bjorken integral at low Q^{*2} . *Phys. Rev. Lett.*, 93:212001, 2004.
- 604 [23] A. Deur et al. Experimental study of isovector spin sum rules. *Phys.*
605 *Rev. D*, 78:032001, 2008.
- 606 [24] Guido Altarelli, Richard D. Ball, Stefano Forte, and Giovanni Ri-
607 dolfi. Determination of the Bjorken sum and strong coupling from
608 polarized structure functions. *Nucl. Phys. B*, 496:337–357, 1997.
- 609 [25] H. Speisberger. HERACLES and DJANGO: Event Generation of
610 ep Interactions at HERA Including Radiative Processes. available
611 on github.com.
- 612 [26] H. Speisberger. HERACLES and DJANGO6: Updates for version
613 4.6.8 - 4.6.10. available on github.com.
- 614 [27] R. Abdul Khalek et al. Science requirements and detector concepts
615 for the electron-ion collider. *Nuclear Physics A*, 1026:122447, Octo-
616 ber 2022.
- 617 [28] J.-L. Zhang et al. Search for e to tau charged lepton flavor violation
618 at the eic with the ecce detector. *Nuclear Instruments and Methods in*
619 *Physics Research Section A: Accelerators, Spectrometers, Detectors and*
620 *Associated Equipment*, 1053:168276, 2023.
- 621 [29] C. Montag. Private communication.
- 622 [30] J. K. Adkins et al. Design of the ECCE Detector for the Electron Ion
623 Collider. 9 2022.
- 624 [31] J. Adam et al. ATHENA detector proposal — a totally hermetic
625 electron nucleus apparatus proposed for IP6 at the Electron-Ion
626 Collider. *JINST*, 17(10):P10019, 2022.
- 627 [32] S. Agostinelli, J. Allison, K. Amako, J. Apostolakis, H. Araujo,
628 P. Arce, M. Asai, D. Axen, S. Banerjee, G. Barrand, F. Behner,
629 L. Bellagamba, J. Boudreau, L. Broglia, A. Brunengo, H. Burkhardt,
630 S. Chauvie, J. Chuma, R. Chytrcek, G. Cooperman, G. Cosmo,
631 P. Degtyarenko, A. Dell’Acqua, G. Depaola, D. Dietrich, R. Enami,
632 A. Feliciello, C. Ferguson, H. Fesefeldt, G. Folger, F. Foppiano,
633 A. Forti, S. Garelli, S. Giani, R. Giannitrapani, D. Gibin, J.J. Gómez
634 Cadenas, I. González, G. Gracia Abril, G. Greeniaus, W. Greiner,
635 V. Grichine, A. Grossheim, S. Guatelli, P. Gumplinger, R. Hamatsu,
636 K. Hashimoto, H. Hasui, A. Heikkinen, A. Howard, V. Ivanchenko,
637 A. Johnson, F.W. Jones, J. Kallenbach, N. Kanaya, M. Kawabata,
638 Y. Kawabata, M. Kawaguti, S. Kelner, P. Kent, A. Kimura, T. Ko-
639 dama, R. Kokoulin, M. Kossov, H. Kurashige, E. Lamanna, T. Lam-
640 p  n, V. Lara, V. Lefebvre, F. Lei, M. Liendl, W. Lockman, F. Longo,
641 S. Magni, M. Maire, E. Medernach, K. Minamimoto, P. Mora
642 de Freitas, Y. Morita, K. Murakami, M. Nagamatsu, R. Nartallo,
643 P. Nieminen, T. Nishimura, K. Ohtsubo, M. Okamura, S. O’Neale,
644 Y. Oohata, K. Paech, J. Perl, A. Pfeiffer, M.G. Pia, F. Ranjard,
645 A. Rybin, S. Sadilov, E. Di Salvo, G. Santin, T. Sasaki, N. Savvas,
646 Y. Sawada, S. Scherer, S. Sei, V. Sirotenko, D. Smith, N. Starkov,
647 H. Stoecker, J. Sulkimo, M. Takahata, S. Tanaka, E. Tcherniaev,
648 E. Safai Tehrani, M. Tropeano, P. Truscott, H. Uno, L. Urban, P. Ur-
649 ban, M. Verderi, A. Walkden, W. Wander, H. Weber, J.P. Wellisch,
650 T. Wenaus, D.C. Williams, D. Wright, T. Yamada, H. Yoshida, and
651 D. Zschesche. Geant4—a simulation toolkit. *Nuclear Instruments*
652 *and Methods in Physics Research Section A: Accelerators, Spectrometers,*
653 *Detectors and Associated Equipment*, 506(3):250–303, 2003.
- 654 [33] T. Adye et al. <https://gitlab.cern.ch/roounfold/roounfold>.
- 655 [34] Ivica Friscic, Dien Nguyen, Jackson Pybus, Alex Jentsch, Efrain
656 Segarra, Mark Baker, Or Hen, Douglas Higinbotham, Richard Mil-
657 ner, Arun Tadepalli, and Jennifer Rittenhouse West. Neutron spin
658 structure from e-3He scattering with double spectator tagging at
659 the electron-ion collider, 2021.
- 660 [35] L. L. Frankfurt and M. I. Strikman. High-Energy Phenomena, Short
661 Range Nuclear Structure and QCD. *Phys. Rept.*, 76:215–347, 1981.
- 662 [36] C. Ciofi degli Atti and L.P. Kaptari. On the interpretation of the pro-
663 cesses He-3(e,e-prime p) H-2 and He-3(e,e-prime p)(pn) at high
664 missing momenta. *Phys. Rev. Lett.*, 95:052502, 2005.
- 665 [37] A. Accardi, L. T. Brady, W. Melnitchouk, J. F. Owens, and N. Sato.
666 Constraints on large-x parton distributions from new weak bo-
667 son production and deep-inelastic scattering data. *Phys. Rev. D*,
668 93(11):114017, 2016.
- 669 [38] A. Accardi and S. Li. private communication.
- 670 [39] A. Bylinkin et al. Detector requirements and simulation results
671 for the eic exclusive, diffractive and tagging physics program us-
672 ing the ecce detector concept. *Nuclear Instruments and Methods in*

- 673 *Physics Research Section A: Accelerators, Spectrometers, Detectors and*
674 *Associated Equipment*, 1052:168238, 2023.
- 675 [40] Nobuo Sato, W. Melnitchouk, S. E. Kuhn, J. J. Ethier, and A. Accardi. Iterative Monte Carlo analysis of spin-dependent parton distributions. *Phys. Rev. D*, 93(7):074005, 2016.
- 676
677
- 678 [41] X. Zheng et al. Precision measurement of the neutron spin asymmetries and spin-dependent structure functions in the valence quark region. *Phys. Rev. C*, 70:065207, 2004.
- 679
680
- 681 [42] K. Abe et al. Measurements of $R = \sigma(L) / \sigma(T)$ for $0.03 < x < 0.1$ and fit to world data. *Phys. Lett. B*, 452:194–200, 1999.
- 682
- 683 [43] R. P. Feynman. Photon-hadron interactions. 1973.
- 684 [44] C. Cocuzza, W. Melnitchouk, A. Metz, and N. Sato. Polarized antimatter in the proton from a global QCD analysis. *Phys. Rev. D*, 106(3):L031502, 2022.
- 685
686
- 687 [45] Robert Fersch et al. Determination of the Proton Spin Structure Functions for $0.05 < Q^2 < 5\text{GeV}^2$ using CLAS. *Phys. Rev. C*, 96(6):065208, 2017.
- 688
689
- 690 [46] M. M. Dalton, A. Deur, C. D. Keith, S. Širca, and J. Stevens. Measurement of the high-energy contribution to the Gerasimov-Drell-Hearn sum rule. 8 2020.
- 691
692
- 693 [47] S. D. Bass and Martina M. Brisudova. The Spin and flavor dependence of high-energy photoabsorption. *Eur. Phys. J. A*, 4:251–258, 1999.
- 694
695
- 696 [48] I. Abt et al. Measurement of jet production in deep inelastic scattering and NNLO determination of the strong coupling at ZEUS. *Eur. Phys. J. C*, 83(11):1082, 2023.
- 697
698
- 699 [49] Sheng-Quan Wang, Stanley J. Brodsky, Xing-Gang Wu, Jian-Ming Shen, and Leonardo Di Giustino. Elimination of QCD Renormalization Scale and Scheme Ambiguities – arXiv [hep-ph]:2302.08153 [hep-ph]. in *Special issue of Universe, “The Quantum Chromodynamics: 50th Anniversary of the Discovery”*, 2 2023.
- 700
701
702
703
- 704 [50] Stanley J. Brodsky, G. Peter Lepage, and Paul B. Mackenzie. On the Elimination of Scale Ambiguities in Perturbative Quantum Chromodynamics. *Phys. Rev. D*, 28:228, 1983.
- 705
706
- 707 [51] Alexandre Deur, Jian-Ming Shen, Xing-Gang Wu, Stanley J. Brodsky, and Guy F. de Teramond. Implications of the Principle of Maximum Conformality for the QCD Strong Coupling. *Phys. Lett. B*, 773:98, 2017.
- 708
709
710
- 711 [52] A. Accardi et al. Strong Interaction Physics at the Luminosity Frontier with 22 GeV Electrons at Jefferson Lab. 6 2023.
- 712
- 713 [53] Salim Cerci, Zuhail Seyma Demiroglu, Abhay Deshpande, Paul R. Newman, Barak Schmookler, Deniz Sunar Cerci, and Katarzyna Wichmann. Extraction of the strong coupling with HERA and EIC inclusive data. *Eur. Phys. J. C*, 83(11):1011, 2023.
- 714
715
716